

# Vector spectral functions and transport properties in quenched QCD

---

## Heng-Tong Ding

*Key Laboratory of Quark & Lepton Physics (MOE) and Institute of Particle Physics, Central China Normal University, Wuhan 430079, China*

*E-mail: [hengtong.ding@mail.ccnu.edu.cn](mailto:hengtong.ding@mail.ccnu.edu.cn)*

## Olaf Kaczmarek

*Fakultät für Physik, Universität Bielefeld, 33615 Bielefeld, Germany*

*E-mail: [okacz@physik.uni-bielefeld.de](mailto:okacz@physik.uni-bielefeld.de)*

## Florian Meyer\*

*Fakultät für Physik, Universität Bielefeld, 33615 Bielefeld, Germany*

*E-mail: [fmeyer@physik.uni-bielefeld.de](mailto:fmeyer@physik.uni-bielefeld.de)*

We present new results on the reconstruction of mesonic spectral functions for three temperatures  $1.1T_c$ ,  $1.2T_c$  and  $1.4T_c$  in quenched QCD. Making use of non-perturbatively improved clover Wilson valence quarks allows for a clean extrapolation of correlator data to the continuum limit. For the case of vanishing momentum the spectral function is obtained by fitting the data to a well motivated ansatz, using the full covariance matrix of the continuum extrapolated data in the fit. We found that vector correlation function is almost temperature independent in the current temperature window. The electrical conductivity of the hot medium, related to the origin of the vector spectral function at zero momentum, is computed from the resulting parameters at all three temperatures, leading to an estimate of  $0.2C_{em} \lesssim \sigma/T \lesssim 0.4C_{em}$ . The dilepton rates resulting from the obtained spectral functions show no significant temperature dependence.

*The 32nd International Symposium on Lattice Field Theory,  
23-28 June, 2014  
Columbia University New York, NY*

---

\*Speaker.

## 1. Introduction

Ongoing Heavy Ion Collision experiments conducted at facilities like RHIC and LHC provide new output about the nature of elementary particles and their interactions. The spectral function in the vector channel at finite temperature provides information on the thermal dilepton rates accessible in those experiments [1, 2], which we will attempt to extract from the fundamental theory of QCD in the following. Important dynamical quantities can be extracted from the inherently non-perturbative regime of small frequencies, which motivates the use of lattice data. With this we extend our former investigations [3, 4, 5]. A typically well accessible quantity on the lattice is the correlation function in a given spectral channel. It inhibits dynamical properties of the QGP state when investigated at finite temperature [6, 7]. As such, the light vector correlator is related to the electrical conductivity  $\sigma$  of the QGP, the dilepton rate  $\frac{dW}{d\omega d^3p}$  and the photon rate  $\frac{dR}{d^3p}$  as measured in heavy ion collision experiments, via its spectral function  $\rho_V$  [8, 9]. While the spectral function relates to the correlator through an integral equation,

$$G_H(\tau, \vec{p}) = \int_0^\infty \frac{d\omega}{2\pi} \rho_H(\omega, \vec{p}, T) K(\omega, \tau, T) \quad \text{with} \quad K(\omega, \tau, T) = \frac{\cosh(\omega(\tau - \frac{1}{2T}))}{\sinh(\frac{\omega}{2T})}, \quad (1.1)$$

the electrical conductivity is related to the spectral function via the Kubo formula,

$$\frac{\sigma}{T} = \frac{C_{em}}{6} \lim_{\omega \rightarrow 0} \frac{\rho_{ii}}{\omega}. \quad (1.2)$$

The two experimentally observable rates are in terms of the spectral function given by

$$\frac{dW}{d\omega d^3p} \sim \frac{\rho_V(\omega, \vec{p}, T)}{(\omega^2 - \vec{p}^2)(e^{\omega/T} - 1)}, \quad \omega \frac{dR_\gamma}{d^3p} \sim \frac{\rho_V^T(\omega = |\vec{p}|, T)}{e^{\omega/T} - 1}. \quad (1.3)$$

These relations imply that once the spectral function of the vector channel is extracted from QCD, important insights into non-perturbative phenomena of heavy ion collisions and the QGP can be gained.

In order to determine the spectral function, however, (1.1) has to be inverted, which is often referred to as an "ill posed" problem [6]. The baseline of this reasoning is that the numerical (temporal) correlator data contains  $\mathcal{O}(10)$  points, while a decent resolution of the spectral function on the other hand requires  $\mathcal{O}(1000)$  points. Thus additional information has to be provided, which we choose to be in the form of a phenomenologically inspired ansatz which is fitted to continuum extrapolated lattice QCD correlation functions.

## 2. Lattice observables and continuum extrapolation

The renormalized isovector correlation function is constructed as

$$J_H = Z_V \bar{\Psi}(x) \gamma_H \Psi(x) \quad \rightarrow \quad G_H(\tau, \vec{x}) = \langle J_H(\tau, \vec{x}) J_H^\dagger(0, \vec{0}) \rangle, \quad (2.1)$$

and projected to definite momentum  $\vec{p}$ :

$$G_H(\tau, \vec{p}) = \sum_{\vec{x}} G_H(\tau, \vec{x}) e^{i\vec{p}\vec{x}}. \quad (2.2)$$

In this study we constrain ourselves to the case  $\vec{p} = 0$ . Splitting the correlation function (2.2) into spatially and temporally polarized components, in Euclidean metric  $G_V = G_{ii} + G_{00}$ , we form a ratio of correlation functions

$$R_{ii} = \frac{T^2}{\chi_q} \frac{G_{ii}(\tau T)}{G_V^{free,lat}(\tau T)}, \quad \chi_q = -G_{00}/T, \quad (2.3)$$

where  $G_{ii}$  is normalized by both the full free correlator on the lattice [13] and the quark number susceptibility  $\chi_q$ . The division by the latter rids us of the need to actually renormalize the spatial current correlator  $G_{ii}$ , while the division by the former cancels its exponential falloff.

|                                | $N_\tau$ | $N_\sigma$ | $\beta$ | $\kappa$ | $1/a[\text{GeV}]$ | # conf. |
|--------------------------------|----------|------------|---------|----------|-------------------|---------|
| $\mathbf{T} = 1.1\mathbf{T}_c$ | 32       | 96         | 7.192   | 0.13440  | 9.65              | 314     |
|                                | 48       | 144        | 7.544   | 0.13383  | 13.21             | 358     |
|                                | 64       | 192        | 7.793   | 0.13345  | 19.30             | 242     |
| $\mathbf{T} = 1.2\mathbf{T}_c$ | 28       | 96         | 7.192   | 0.13440  | 9.65              | 232     |
|                                | 42       | 144        | 7.544   | 0.13383  | 13.21             | 417     |
|                                | 56       | 192        | 7.793   | 0.13345  | 19.30             | 273     |
| $\mathbf{T} = 1.4\mathbf{T}_c$ | 24       | 128        | 7.192   | 0.13440  | 9.65              | 340     |
|                                | 32       | 128        | 7.457   | 0.13390  | 12.86             | 255     |
|                                | 48       | 128        | 7.793   | 0.13340  | 19.30             | 456     |

**Table 1:** Parameters of all lattices for all temperatures used in this study.

Lattice calculations have been performed using a non-perturbatively improved Wilson-Clover action without dynamical sea quarks at three different temperatures  $T = 1.1T_c, 1.2T_c$  and  $1.4T_c$  with 3 increasingly finer lattices each, see Tab. 1. All valence quark masses are chosen to be small around  $m_{\overline{MS}}(\mu = 2\text{GeV}) \sim \mathcal{O}(10\text{MeV})$ . Note that for the two lowest temperatures the aspect ratio is fixed to  $N_s/N_t = 3$  and  $N_s/N_t = 3.42$ , respectively, ensuring a constant physical volume, while for the  $T = 1.4T_c$  lattice finite volume effects were verified to be small [3].

For all three temperatures continuum extrapolations have been performed in  $a^2$  for all  $N_\tau/2$  original distances available on the finest lattice. To achieve this, corresponding data points on the coarser lattices have been spline interpolated along  $\tau T$ . The result is shown, for  $T = 1.1T_c$ , in Fig. 1 (*left*). The errors on the continuum extrapolated ratios obtained from a bootstrap analysis are slightly below the one percent level. The continuum extrapolated correlation functions  $G_{ii}/T^3$  for each temperature are shown in in Fig. 1 (*right*). The correlators overlap, thus we expect the same scaling with temperature in our resulting spectral functions, already indicating that temperature effects in the dilepton rates and the electrical conductivities seem to be small.

### 3. Fitting to the data

In order to extract the vector spectral function via (1.1) we employ an ansatz for its spatial

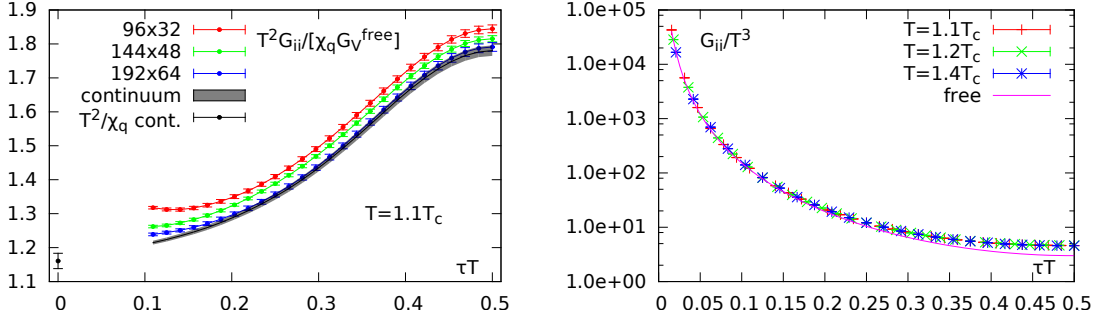


**Figure 1:** *Left:* All three lattice correlators and the resulting continuum extrapolated correlator for the  $T = 1.1T_c$  dataset. Note that the finest lattice agrees with the continuum extrapolation down to  $\tau T \sim 0.18$ . The datapoint at  $\tau T = 0$  indicates the continuum extrapolated result for the inverted quark number susceptibility. *Right:* Continuum extrapolated correlation functions for all three temperatures. Shown are the renormalized spatial components. The solid line is the corresponding free correlation function.

part:

$$\rho_{ii}(\omega, T) = \chi_q c_{\text{BW}} \frac{\omega \Gamma}{\omega^2 + (\Gamma/2)^2} + \frac{3}{2\pi} (1+k) \omega^2 \tanh\left(\frac{\omega}{4T}\right) \quad (3.1)$$

$$\equiv \rho_{\text{BW}}(\omega, T) + (1+k) \rho_V^{\text{free}}(\omega, T). \quad (3.2)$$

It consists of two parts: a Breit-Wigner peak, corresponding to the low  $\omega$  region, and a modified version of the free spectral function. The modification parameter in the latter case fulfills  $k = \alpha_s/\pi$  at leading order perturbation theory [3]. This ansatz is inspired by the known relations for spectral functions in the non-interacting case,

$$\rho_{ii}^{\text{free}}(\omega, T) = 2\pi T^2 \omega \delta(\omega) + \frac{3}{2\pi} \omega^2 \tanh\left(\frac{\omega}{4T}\right), \quad \rho_{00}^{\text{free}}(\omega, T) = 2\pi T^2 \omega \delta(\omega) \quad (3.3)$$

$$\text{and } \rho_V^{\text{free}}(\omega, T) = \rho_{ii}^{\text{free}}(\omega, T) - \rho_{00}^{\text{free}}(\omega, T). \quad (3.4)$$

While the temporal correlator is constant due to charge conservation, and thus the  $\delta$ -function in its spectral function is protected by symmetry, the corresponding  $\delta$ -function in the spatial part is expected to be washed out upon the onset of interactions [7, 9, 10]. This effect is hence modeled as a Breit-Wigner peak in our ansatz.

An estimator for this spectral function is then obtained from relation (1.1) by  $\chi^2$ -minimizing the ansatz on the r.h.s. with respect to the continuum extrapolated ratio data from eqn. (2.3) on the l.h.s. The fit itself is fully correlated with the covariance matrix of the extrapolated continuum data estimated from the bootstrap samples. From the entries of the covariance matrix it becomes apparent that there are covariances between data points used in the fit, which are comparable in size to the variances of the data at and around the midpoint, and hence non-negligible in the construction the  $\chi^2$  function.

However, the information about the small  $\omega$  region resides in the large  $\tau T$  region of the correlator [11], i.e. around its midpoint. In order to extract more information from this region we also extract and fit the first thermal moment of the correlator, see e.g. [3] for a detailed discussion.

## 4. Results

In the following our procedure is shown using  $T = 1.1T_c$  as an example case. The fits of the ansatz (3.1) to the continuum extrapolated data show a very good convergence behaviour and yield as a result the three fit parameters  $\Gamma$ ,  $c_{BW}$ ,  $k$  and their respective statistical fit errors, see the first column of Tab. 2. In Fig. 1 (left) one sees that the ratio on the finest lattice agrees with the continuum above  $\tau T \simeq 0.18$ , while cutoff effects are visible for the coarser lattices also at larger distances. Although the continuum extrapolation seems to work also for smaller distances, we are careful and include only those  $\tau T$  in the fit where the finest lattice agrees with the continuum extrapolation. Generally, the smallest  $\tau T$  to include in the fit for all temperatures lies in the interval  $[0.18, 0.20]$ . The value of  $\chi^2/\text{dof} = 1.24$  shows that the (rather simple) ansatz describes the data already well. The relative statistical fit errors of the parameters are roughly 30% for  $c_{BW}/\Gamma$  and 40% for  $\Gamma$ . Note that the former has been calculated taking into account the correlation of the two parameters. Using these parameters and their correlation matrix we construct the resulting spectral

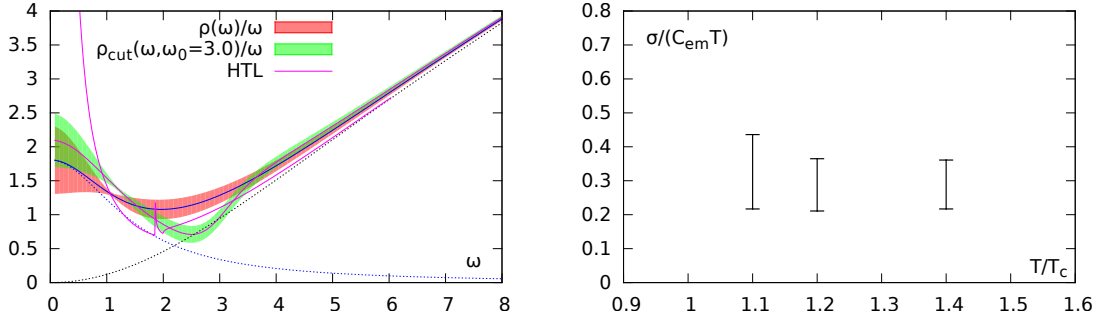


**Figure 2:** *Left:* The spectral functions resulting from the fit for  $T = 1.1T_c$ . The dotted lines are the Breit-Wigner and the free contributions separately to guide the eye. *Right:* The final results for the electrical conductivity for all three temperatures. Their numerical values are listed in Tab. 3.

function with its corresponding statistical errorband in Fig. 2 (left). The electrical conductivity is then obtained from the origin of the spectral function via the Kubo relation (1.2),

$$\frac{\sigma}{C_{em}T} = \frac{2}{3T} \chi_q \frac{c_{BW}}{\Gamma}. \quad (4.1)$$

In order to investigate a possible systematic uncertainty, we introduce a low-frequency cutoff in the free part of the ansatz [3],

$$\rho_V^{\text{free}} \rightarrow \rho_V^{\text{free}} \theta(\omega_0, \Delta_\omega) \quad \text{with} \quad \theta(\omega_0, \Delta_\omega) = \left(1 + \exp((\omega_0^2 - \omega^2)/(\omega\Delta_\omega))\right)^{-1}, \quad (4.2)$$

with  $\theta(\omega_0, \Delta_\omega)$  being a representation of the  $\theta$ -function for  $\Delta_\omega = 0$ , and smeared out for  $\Delta_\omega \neq 0$ . Effectively, by varying  $\omega_0$ , we probe the sensitivity of our Ansatz with respect to a continuous change in the low frequency region, i.e. the free part contributing only for  $\omega \gtrsim \omega_0$ , as opposed to contributing for  $\omega > 0$ . The results for a number of cuts with different  $\omega_0$  applied in the fit procedure is shown in Tab. 2. A value of  $\Delta_\omega/T = 0.5$  is used throughout the scan; the results are insensitive to its actual choice. The results for  $c_{BW}T/\Gamma \sim \sigma$  are rising slightly when moving the cut

| $\Delta_\omega/T$        | 0.0        | 0.5        |            |            |            |            |
|--------------------------|------------|------------|------------|------------|------------|------------|
| $\omega_0/T$             | 0.0        | 1.0        | 2.5        | 3.0        | 3.5        | 4.0        |
| $\Gamma/T$               | 2.89(1.12) | 2.85(1.09) | 2.99(0.95) | 3.31(0.91) | 3.88(0.88) | 4.75(0.88) |
| $\frac{c_{BW}T}{\Gamma}$ | 0.524(146) | 0.543(149) | 0.607(138) | 0.610(115) | 0.595(88)  | 0.571(44)  |
| $k$                      | 0.039(7)   | 0.039(7)   | 0.038(7)   | 0.038(7)   | 0.037(7)   | 0.035(7)   |
| $\chi^2/\text{dof}$      | 1.24       | 1.24       | 1.23       | 1.22       | 1.21       | 1.19       |

**Table 2:** Fit results for  $T = 1.1T_c$  and some selected cutoffs. Note that  $c_{BW}/\Gamma$  is directly proportional to the electrical conductivity  $\sigma$ .

to higher frequencies, showing that the peak rises in height. Around  $\omega_0/T \simeq 3$  the peak becomes much broader to compensate for the cut off contribution and  $c_{BW}T/\Gamma$  falls off again. At this point the Breit-Wigner peak contributes (as the only contribution) to a frequency regime that is, for the uncut fit, already dominated by the free part, see Fig. 2. Raising  $\omega_0/T$  even further does, from a physical point of view, not make sense anymore. In addition, note how the value of  $\chi^2/\text{dof}$  is not rising although the procedure: a-priori there is no reason for the fit to become much worse, in terms of its  $\chi^2$  value, upon the application of such cuts. It turns out the ansatz can perfectly compensate for the missing free contribution to the extent of  $\omega_0/T \simeq 3$ . Beyond that, mathematically the Breit-Wigner peak can still compensate for the cut, but, as argued above, the initial physical motivation of this form of ansatz is not given anymore.

| $T$   | $1.1T_c$ | $1.2T_c$ | $1.4T_c$ |
|---|----------|----------|----------|
| $\left(\frac{\sigma}{c_{em}T}\right)_{max}$ | 0.436    | 0.365    | 0.361    |
| $\left(\frac{\sigma}{c_{em}T}\right)_{min}$ | 0.217    | 0.211    | 0.217    |

**Table 3:** Final results for the electrical conductivity. Note that the systematic error from the cut-procedure and the statistical fit error are included (see text).

For the electrical conductivity, however, we can include its maximal deviation from the uncut result as an upper systematical error. Our results for the electrical conductivity for all three temperatures are given in Tab. 3 and Fig. 2 (right), respectively. They are comparable to recent studies [14, 15] using MEM and Wilson Clover fermions at finite lattice spacing. For a comparison of different calculations of the electrical conductivity see [12]. The thermal dilepton rates calculated from our ansatz for the spectral functions via the first expression of (1.3) are shown in Fig. 3 for all three temperatures. They are qualitatively comparable to the rate obtained by an HTL calculation [16] in the intermediate  $\omega$  region, as well as to the leading order (Born) rate for large  $\omega$ . However, our results show a better behaviour for small  $\omega$  consistent with a finite electrical conductivity (see also Fig. 2 (left)).

## 5. Conclusion

Using non-perturbatively improved Wilson Clover valence fermions we performed continuum extrapolations of light vector channel correlation functions. The extrapolations yield reliable results

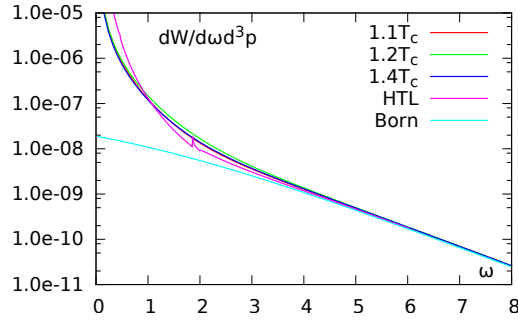


**Figure 3:** The thermal dilepton rate as a function of  $\omega$ .

with errors at the sub-percent level. Employing an ansatz for the corresponding spectral function, these are used to perform a fully correlated  $\chi^2$ -minimization and to obtain results for the spectral functions and the electrical conductivities via a Kubo relation. The electrical conductivities are in accordance with earlier results obtained by MEM and  $\chi^2$ -minimization methods. The thermal dilepton rates are obtained and compared to the HTL and leading order rates and show almost no thermal effect in the analyzed temperature region.

**Acknowledgements:** The results have been achieved using the PRACE Research Infrastructure resource JUGENE based at the Jülich Supercomputing Centre in Germany and the Bielefeld GPU-cluster resources. This work has been partly supported by BMBF under grants 05P12PBCTA and 56268409 and the GSI BILAER grant.

## References

- [1] R. Rapp, et. al., in *Landolt-Börnstein*, vol. I-23, 4-1. Springer-Verlag, 2010.
- [2] D. Bernecker, H. B. Meyer, *Eur.Phys.J.* **A47** (2011) 148.
- [3] H.-T. Ding et al., *Phys.Rev.* **D83** (2011) 034504.
- [4] A. Francis, O. Kaczmarek, *Prog.Part.Nucl.Phys.* **67** (2012) 212.
- [5] O. Kaczmarek, M. Müller, *PoS LATTICE2013* (2013) 175
- [6] H. B. Meyer, *Eur.Phys.J.* **A47** (2011) 86
- [7] J. Hong, D. Teaney, *Phys.Rev.* **C82** (2010) 044908.
- [8] L. D. McLerran and T. Toimela, *Phys. Rev.* **D31** (1985) 545.
- [9] G. D. Moore, J.-M. Robert, (2006), hep-ph/0607172.
- [10] G. Aarts, J. M. Martinez Resco, *JHEP* **0204** (2002) 053
- [11] G. Aarts, J. M. Martinez Resco, *Nucl.Phys.Proc.Suppl.* **119** (2003) 505
- [12] C. Greiner et. al., *Phys.Rev.* **C83** (2011) 014908.
- [13] F. Karsch et al., *Phys. Rev.* **D68** (2003) 014504
- [14] B. B. Brandt et al., *JHEP* **1303** (2013) 100.
- [15] A. Amato et al., *Phys. Rev. Lett.* **111** (2013) 172001.
- [16] E. Braaten, R. D. Pisarski, *NP* **B337** (1990) 569